Pre-main-sequence accretion of low-mass stars in the `Cesam2k20` code

Student
Ducheng Lu

Supervisors
Dr. Ludovic Petitedemange
Dr. João Pedro Cadilhe Marques
Dr. Louis Manchon
Dr. Charly Pinçon

June 2025

Contents

1 Introduction **1**

2 Pre-main-sequence accretion **2**
2.1 Pre-main-sequence magnetospheric accretion 2
2.2 Observational evidence of magnetospheric accretion . . . 3

3 Stellar evolution modeling **4**
3.1 Stellar structure equations 4
3.2 Pre-main-sequence evolution 6

4 Methods **6**
4.1 Modeling the consequences of accretion 6
4.1.1 Deuterium burning 6
4.1.2 Hot and cold accretion 6
4.2 The stellar evolution code `Cesam2k20` 6
4.2.1 Lagrangian variables 6
4.2.2 Automatic allocation of grid points 7
4.2.3 Structure equations 7
4.2.4 Input physics 8
4.3 Accretion in `Cesam2k20` 9
4.3.1 Limiting the maximum change in gravitational energy 9
4.3.2 Limiting the maximum change in mass 9

5 Results **9**
5.1 The toy problem 9
5.2 The effect of different accretion rates 9
5.3 The effect of different chemical compositions 9
5.4 Comparison with Palla & Stahler (1993) 9

6 Conclusion **9**

References **11**

A Appendix: The jacobian of the stellar structure equations **14**

Abstract

Context.
Aim.
Methods.
Results.

Abstract

Contexte.
Objectif.
Méthodes.
Résultats.

1 Introduction

Stars form through the gravitational collapse of dense cores within molecular clouds. Initially, this collapse is isothermal, with temperature remaining nearly constant. As the density increases, the central region becomes increasingly opaque to radiation, inhibiting its escape from the core while still allowing it from the outer layers. This increase in opacity leads to an adiabatic collapse of the center, during which the temperature and pressure rise until a hydrostatic core, or a protostar, is formed. The protostar then accretes material from the surrounding cloud, a process that can continue for several million years.

Once most of the surrounding material has been accreted, the protostar enters the pre-main-sequence (PMS) phase and becomes visible as a T Tauri star (TTS). TTSs are late-type PMS stars that serve as precursors to low-mass main-sequence stars. Classical T Tauri stars (CTTSs) are characterized by strong infrared (IR) emission from their optically thick accretion disks. As accretion declines due to the depletion of material in the inner disk, the IR emission weakens, and the stars are then observed as weak T Tauri stars (WTTSs). Young massive stars are also expected to undergo accretion during their early evolution and are observed as Herbig Ae/Be stars—hotter and more luminous than TTSs. However, the accretion processes for these higher-mass stars remain poorly understood.

The earliest accretion stages remain observationally elusive, as protostars are deeply embedded in the surrounding dusty cloud, making it highly extincted in optical and near-IR wavelengths. Nonetheless, indirect indicators such as disks, outflows, and jets provide compelling evidence of ongoing accretion. Modeling these stages remains challenging due to the time-variable, non-linear nature of the process and the complexity of the underlying physics.

When Henyey et al. (1955) and Hayashi (1961) first studied the early phases of stellar evolution, accretion was not taken into account. Instead, stars were assumed to begin their evolution as fully convective objects with very large radii and luminosities, contracting under their own gravity until a radiative core developed, eventually reaching the main sequence. These evolutionary paths are now known as the Hayashi and Henyey tracks. Since Larson (1969) introduced the concept of the formation of a hydrostatic core, followed by continued accretion from an infalling envelope of gas and dust, accretion has been recognized as a fundamental process in early stellar evolution, supported by both theoretical and observational studies.

There has been growing interest in studying accretion in PMS stars, particularly because of its relevance to planetary formation. Accretion disks are the birthplaces of planets and other small bodies, making the study of accretion crucial for understanding the early evolution of planetary systems. Beyond this, accretion can significantly influence the internal structure and rotation of stars by supplying both mass and angular momentum. These structural and rotational changes can, in turn, affect the stellar dynamo mechanism responsible for amplifying magnetic fields in young stars (e.g., Stelzer and Neuhäuser 2001).

Accretion also impact long-term stellar evolution by setting the initial conditions for subsequent evolutionary stages and can leave lasting imprints. In addition, accretion can alter the surface chemical composition, especially if the accreted material differs in abundance from that of the protostar (Kunitomo and Guillot 2021). This has important implications for interpreting observed stellar abundances and for modeling chemical mixing processes.

Finally, accretion history plays a critical role in understanding young stellar clusters. It can influence the shape of the initial mass function, contribute to the observed luminosity spread among cluster members, and affect the positioning of stars on theoretical isochrones (Baraffe et al. 2009, 2012; Hosokawa et al. 2011). Accurate modeling of accretion is therefore important for interpreting observed features of young clusters.

In this project, we investigate the impact of accretion on stellar structure and evolution using the `Cesam2k20` version of the 1D stellar evolution code *Code d'Évolution Stellaire Adaptatif et Modulaire* (`CESAM`) (Marques et al. 2013; Morel 1997; Morel and Lebreton 2008). Our goal is to implement accretion in `Cesam2k20`, which will allow us to examine its effects on stellar evolution and structure, and to compare the results with theoretical predictions and other stellar evolution models.

This study focuses on the later stages of the accretion process, after the formation of a hydrostatic core. We restrict our analysis to low-mass stars, as accretion in high-mass stars remains less constrained and falls outside the scope of this work.

A parallel branch of the original `CESAM` code, *Code d'Évolution Planétaire Adaptatif et Modulaire* (`CEPAM`) (Guillot and Morel 1995), has been developed for modeling planetary formation and evolution. A future unification of these two branches would provide a powerful framework for studying the coupled evolution of stars and their planetary systems.

In the next section, we review the current understanding of pre-main-sequence accretion, including the mechanisms of magnetospheric accretion and a brief overview of the observational evidence supporting it. Sec.3 presents the fundamental equations governing stellar structure and outlines how pre-main-sequence evolution is modeled in stellar evolution codes. In Sec.4, we begin by discussing the modeling of the consequences of accretion, followed by a description of the `Cesam2k20` code, including its numerical structure and input physics. We then detail the implementation of accretion in the code. The results of our models are presented in Sec.5, where we explore the effects of different accretion rates and deuterium abundances, and compare our findings with previous work by Palla and Stahler (1993). Finally, Sec.6 summarizes our main findings, discusses the limitations of the current work, and outlines future prospects.

2 Pre-main-sequence accretion

In this section, we will review the current understanding of stellar accretion, including the mechanisms of magnetospheric accretion and the observational evidence for accretion in pre-main-sequence stars.

2.1 Pre-main-sequence magnetospheric accretion

Stellar magnetic fields play a crucial role in the accretion of pre-main-sequence stars, through the mechanism known as magnetospheric accretion (See, for example, Hartmann et al. 2016, for a review).

Fig. 1 is a schematic illustration of magnetospheric accretion onto young ($1 \lesssim t \lesssim 10,$ Myr), low-mass ($\lesssim 1 M_{\odot}$) stars. The strong stellar magnetic field truncates the circumstellar disk at a few stellar radii. The dust disk is truncated slightly farther out than the gas disk, as dust in the inner disk sublimates due to heating by the stellar radiation field. The inner edge of the dust disk is responsible for most of the observed near-IR excess. Material from the disk is funneled onto the star along the magnetic field lines, where it is heated to approximately 10^4, K, producing broad emission lines. The accretion flow is accelerated along the field lines, eventually reaching the stellar surface at nearly free-fall velocity. This process leads to the formation of an accretion shock at the stellar surface, where the gas is briefly halted and heated to very high temperatures, emitting

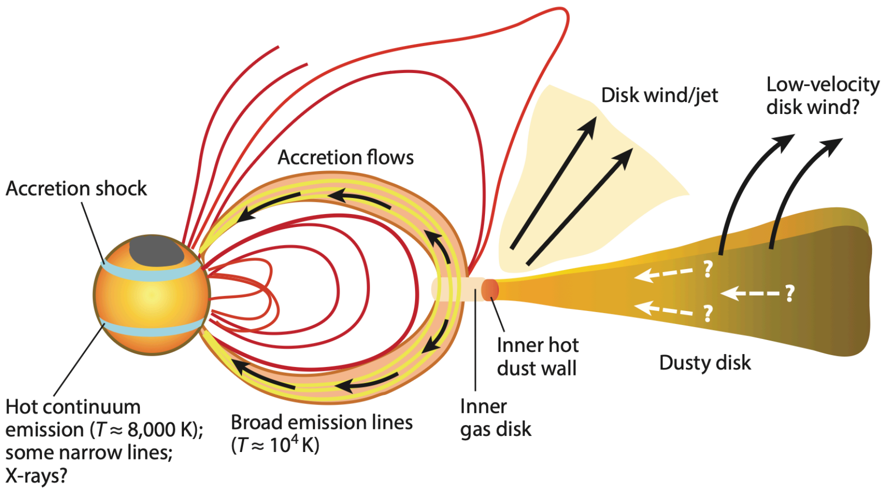

Figure 1: Schematic illustration of magnetospheric accretion onto young low-mass stars. The strong stellar magnetic field truncates the circumstellar disk at a few stellar radii. Accreting material is channeled along the magnetic field lines and impacts the stellar surface, forming an accretion shock. Jets and disk winds may also play a role in the star-disk interaction. The exact mechanisms for mass and angular momentum transport in the star-disk system remain uncertain. The figure is reproduced from Fig. 1 of Hartmann et al. (2016).

X-rays. Most of these X-rays are absorbed and reradiated in the ultraviolet and optical continuum.

Despite recent advances in the study of magnetospheric accretion, many aspects are still under debate. Bouvier (2014) summarizes several open issues regarding the physics of the magnetospheric accretion and ejection processes. One of the long-standing problems is the evolution of stellar rotation: while the angular momentum carried by accreting material should spin up the star, observations reveal that the rotation rates of PMS stars are lower than expected. This discrepancy suggests that some form of magnetic braking must be at work to regulate stellar spin (e.g., Herbst et al. 2007).

Magnetohydrodynamic simulations suggest that jets, disk winds, and magnetospheric ejections are involved in removing angular momentum during accretion (e.g., Ireland et al. 2020; Lii et al. 2014; Romanova et al. 2004). However, the relative importance of these mechanisms in shaping the angular momentum evolution remains under investigation(e.g., Kunitomo et al. 2017). Although the models presented in this work do not include magnetic fields or rotation, understanding the broader framework of magnetospheric accretion is essential for interpreting how accretion affects stellar structure. Including these physical processes for more realistic accretion modeling will be an important direction for future work.

2.2 Observational evidence of magnetospheric accretion

Observations of CTTSs provide strong evidence for magnetospheric accretion, including the presence of strong stellar magnetic fields, an inner cavity of a few stellar radii within the magnetosphere, magnetic accretion columns filled with free-falling plasma, and accretion shocks at the stellar surface.

The accretion shock produces emission in the ultraviolet, optical, and near-infrared wavelengths, as well as a modest amount of X-rays. These emissions serve as crucial diagnostics of the accretion region, allowing measurements of the accretion luminosity which, when combined with stellar mass and radius, provide estimates of accretion rates. Soft X-ray emission, unique to accreting stars, has also been detected from CTTSs and is likely produced in the post-shock region (e.g., Kastner et al. 2002). Magnetospheric accretion flows can be identified by redshifted absorption features in specific spectral lines (Muzerolle et al. 2001), while blueshifted forbidden emission lines have been linked to strong winds and mass outflows (e.g., Bally 2016).

Magnetospheric accretion paradigm assumes that the stellar magnetic field is strong enough to counteract the pressure of the accretion disk and disrupt the disk before it reaches the stellar surface (e.g., Koenigl 1991). At the truncation radius $R_{\rm trunc}$, the magnetic pressure approximately balances the gas ram pressure, i.e., $B^2/8\pi \simeq \frac{1}{2}\rho v^2$, where the relevant velocity is roughly the Keplerian velocity, $v = \sqrt{GM_\star/R_{\rm trunc}}$. The exact location of this truncation radius will also depend on the accretion rate (see Eq. 2.2 in Bouvier et al. 2007). This framework generally aligns with the measured magnetic field strengths of CTTSs, which typically range from a few hundred Gauss to a few kiloGauss (Alencar et al. 2012; Bouvier et al. 2007).

3 Stellar evolution modeling

Stellar evolution modeling involves combining physical principles with numerical methods to simulate how stars change over time. This section first introduces the fundamental equations that describe stellar evolution and then turns the focus to the modeling of pre-main-sequence stars.

3.1 Stellar structure equations

Modeling stellar evolution involves defining initial conditions and solving the differential equations that govern the physical processes inside a star, thereby predicting how stellar properties change over time. The primary factors determining a star's evolution are its mass and initial chemical composition. Once specified, these initial parameters are input into the stellar structure equations, which express the characteristic stellar properties (e.g., pressure P, temperature T, luminosity L, density ρ) as functions of position and time $(\vec{r}, t)$. By assuming spherical symmetry, the position can be reduced to the radial distance r from the center, so physical quantities become functions of radius and time, i.e., (r, t).

During stellar evolution, the total stellar mass remains almost constant except in cases of significant mass loss. In contrast, the stellar radius may vary rapidly as the star goes into different stages. Therefore, it is more convenient to introduce a Lagrangian coordinate m (defined as the total mass inside the sphere of radius r) instead of r.

In the mass coordinate, the system of 1D stellar structure equations can be written as

(See, for example, Kippenhahn et al. 2013):

$$\frac{\partial p}{\partial m} = -\frac{Gm}{4\pi r^2} + \frac{\Omega}{6\pi r^2}, \tag{1a}$$
$$\frac{\partial T}{\partial m} = \frac{\partial p}{\partial m}\frac{T}{p}\nabla, \tag{1b}$$
$$\frac{\partial r}{\partial m} = \frac{1}{4\pi r^2 \rho}, \tag{1c}$$
$$\frac{\partial l}{\partial m} = \epsilon_{\text{nuc}} + \epsilon_\nu + \epsilon_{\text{g}}, \tag{1d}$$
$$\frac{\partial X_i}{\partial t} = -\frac{\partial F_i}{\partial m} + \Psi_i(P, T, \boldsymbol{X}), 1 \leq i \leq n_{\text{elem}}. \tag{1e}$$

where G is the gravitational constant, $\nabla \equiv \partial \ln T / \partial \ln P$ is the temperature gradient, ϵ_{nuc} is the rate of nuclear energy release, ϵ_ν is energy loss rate due to neutrinos escaping from the star, ϵ_{g} is the gravitational energy, X_i is the abundance of the chemical element i, F_i is the flux of the chemical element i due to diffusion, $\boldsymbol{X} \equiv \{X_i\}$ is the chemical composition vector, Ψ_i is the rate of change of X_i by thermonuclear reactions, and n_{elem} is the total number of chemical species considered. All quantities ($p, l, \rho, T, \epsilon, \epsilon_\nu$, etc.) are evaluated locally at each stellar layer.

Eq. (1a) describes the hydrostatic equilibrium and Eq. (1c) describes the mass continuity. Eq. (1d) and Eq. (1b) describe the energy production and energy transport, respectively. These equations illustrate a close coupling between stellar structure and the process of energy production and transport. In most stars, energy is primarily transported by radiation and convection, and the value of ∇ depends on the dominant mechanism of energy transport. Eq. (1e) describes the evolution of the chemical composition of the star, which is governed by the nuclear reactions occurring in the star and the transport of chemical elements. This set of equations assumes spherical symmetry and does not account for magnetic fields, and rotation is included in the centrifugal term in Eq. (1a). These are common simplifications in 1D stellar models and are sufficient for many evolutionary studies.

Stellar evolution is typically treated as a one-dimensional boundary value problem with initial conditions given by the initial mass and chemical composition of the star. The boundary conditions are set at the center and surface of the star. Spherical symmetry requires that the radius, luminosity, and chemical element fluxes vanish at the center of the star. Therefore, we impose:

$$r(0,t) = 0,\ l(0,t) = 0,\ F_i(0,t) = 0, i = 1, \ldots, n_{\text{elem}}. \tag{2}$$

At the surface, the pressure and temperature are set to the values at the base of the stellar atmosphere:

$$p(M_\star, t) = p_{\text{atm}}(L_\star, R_\star, t),\ T(M_\star, t) = T_{\text{atm}}(L_\star, R_\star, t), \tag{3}$$

where $M_\star$, $L_\star$, and $R_\star$ are the stellar mass, luminosity, and radius, respectively. The values of p_{atm} and T_{atm} are derived from reconstruction of the stellar atmosphere, which typically uses empirical relations. As this project focuses on internal structure, we will not delve into the specifics of atmospheric modeling.

With both central and surface boundary conditions specified, and the evolution equations defined in Lagrangian coordinates, the stellar structure problem becomes a well-posed initial-boundary value problem. This framework serves as the basis for numerical stellar evolution codes, which solve these equations to track the stellar evolution over time.

The solutions to the stellar structure equations yield key observable properties of stars, mostly notably their luminosity L and effective surface temperature T_{eff}. These two parameters define a star's position on the Hertzsprung-Russell (HR) diagram, a fundamental tool in astrophysics to understand and visualize stellar evolution. The HR diagram helps to reveal distinct evolutionary stages such as the pre-main-sequence, main sequence, and giant branch, offering a simple way to compare models with observations.

However, translating the underlying physics into stellar models is a complex task. In practice, stellar evolution codes can differ substantially in their model initialization methods. These differences can lead to notable variations during the early evolutionary stages, which will be discussed in the Sec. 3.2. Additionally, variations in the formulations and physical assumptions adopted by these codes influence the predicted stellar properties, often resulting in discrepancies between models. Therefore, it is crucial to carefully consider the specific implementations and assumptions of each code when interpreting stellar evolution results. The details of our physical inputs will be discussed in Sec. 4.2.

3.2 Pre-main-sequence evolution

4 Methods

4.1 Modeling the consequences of accretion

4.1.1 Deuterium burning

4.1.2 Hot and cold accretion

4.2 The stellar evolution code `Cesam2k20`

We use the stellar evolution code `Cesam2k20` (Marques et al. 2013; Morel 1997; Morel and Lebreton 2008) to model stellar evolution with accretion. `Cesam2k20` is a one-dimensional stellar evolution code that employs a spectral method to solve the stellar structure equations given in Eqns. (1). The following subsections describe its numerical implementation, including the choice of variables, the automatic grid-point allocation, the formulation of the structure equations, and the adopted input physics.

4.2.1 Lagrangian variables

The system of equations in Eqns. (1) encapsulates the fundamental physics governing stellar structure and evolution. However, in numerical implementation, these equations are often reformulated to improve stability and convergence. One effective approach, discussed by Morel (1997), is to use the set of variables introduced by Eggleton (1971),

$$\left(\frac{m}{M_\odot}\right)^{2/3}, \quad \left(\frac{r}{R_\odot}\right)^{2}, \quad \left(\frac{L_r}{L_\odot}\right)^{2/3}, \quad L_r \geq 0^{1}.$$

This choice improves numerical precision and helps avoid singularities at the stellar center

[1] In cases where $L_r < 0$—which can occur during late evolutionary stages—the variable $L_r/L_\odot$ is used instead. Since this project focuses on the pre-main-sequence phase, where such cases do not arise, we adopt the Eggleton variables throughout.

Additionally, because pressure and temperature can span several orders of magnitude in the stellar interior, it is numerically advantageous to work with their logarithms. Accordingly, the set of variables ultimately used in `Cesam2k20` is:

$$\xi = \ln P, \quad \eta = \ln T, \quad \zeta = \left(\frac{r}{R_\odot}\right)^2, \quad \lambda = \left(\frac{L_r}{L_\odot}\right)^{2/3}, \quad \mu = \left(\frac{m}{M_\odot}\right)^{2/3}. \tag{4}$$

4.2.2 Automatic allocation of grid points

To resolve the large variations in physical quantities during stellar evolution, an adaptive grid is necessary. To achieve automatic allocation, `Cesam2k20` uses a strictly monotonic spacing function, $Q(\mu, t)$, to distribute grid points based on local physical conditions. Grid points are placed such that the difference in $Q(\mu, t)$ between adjacent points is equal to a time-dependent spacing constant $\psi(t)$ (Eggleton 1971; Morel 1997; Press et al. 1992).

Formally, at each time step t, the grid points $\mu_i,\ i = 1, \ldots, n$ are allocated such that:

$$Q(\mu_{i+1}, t) - Q(\mu_i, t) = \psi(t), \quad i = 1, \ldots, n-1, \tag{5}$$

where $\psi(t)$ is determined during the numerical integration.

The specific form of the spacing function $Q(\mu, t)$ used in `Cesam2k20` is:

$$Q(\mu, t) = -\xi + 15\mu. \tag{6}$$

See Manchon (2021) and Morel (1997) for the rationale behind this choice. The dependence of $Q(\mu, t)$ on pressure (ξ) and mass (μ) ensures finer resolution in regions of steep pressure and density gradients. In the core, where the pressure gradient is modest, resolution is primarily controlled by mass change; while in the outer envelope, where pressure varies rapidly, the grid is refined mostly based on pressure changes.

To map physical coordinates onto the numerical grid, `Cesam2k20` defines an index function $q(\mu, t)$, which takes integer values from 1 to n. The derivative of Q with respect to this index gives:

$$\left.\frac{\partial Q}{\partial q}\right|_t = \left.\frac{\partial Q}{\partial \mu}\right|_t \left.\frac{\partial \mu}{\partial q}\right|_t = \theta(\mu, t) \left.\frac{\partial \mu}{\partial q}\right|_t = \psi(t), \tag{7}$$

where $\theta(\mu, t)$ is directly obtained from the analytic form of $Q(\mu, t)$ in Eq. (6).

The introduction of $\psi(t)$ and $\theta(\mu, t)$ requires two additional equations for closure:

$$\frac{\partial \mu}{\partial q} = \frac{\psi}{\theta}, \quad \frac{\partial \psi}{\partial q} = 0. \tag{8}$$

The first equation relates the mass coordinate to grid index, while the second enforces constant spacing in Q-space. This approach enables efficient resolution of the stellar structure, especially during rapid evolutionary phases.

4.2.3 Structure equations

With the variables introduced in Secs. 4.2.1 and 4.2.2, the stellar structure equations can be expressed in a form more suitable for integration on an equidistant grid in the numerical index $q_i = 1, \ldots, n$.

The full set of structure and composition equations solved at each time step is:

$$0=\frac{\partial\xi}{\partial q}-\left[-\frac{3G}{8\pi}\left(\frac{M_\odot}{R_\odot}\right)^2\left(\frac{\mu}{\zeta}\right)^2+\frac{M_\odot}{4\pi R_\odot}\left(\frac{\mu}{\zeta}\right)^{1/2}\Omega^2\right]e^{-\xi}\frac{\psi}{\theta}, \tag{9a}$$

$$0=\frac{\partial\eta}{\partial q}-\left[-\frac{3G}{8\pi}\left(\frac{M_\odot}{R_\odot}\right)^2\left(\frac{\mu}{\zeta}\right)^2+\frac{M_\odot}{4\pi R_\odot}\left(\frac{\mu}{\zeta}\right)^{1/2}\Omega^2\right]e^{-\xi}\frac{\psi}{\theta}\nabla, \tag{9b}$$

$$0=\frac{\partial\zeta}{\partial q}-\frac{3}{4\pi}\frac{M_\odot}{R_\odot^3}\frac{1}{\rho}\left(\frac{\mu}{\zeta}\right)^{1/2}\frac{\psi}{\theta}, \tag{9c}$$

$$0=\frac{\partial\lambda}{\partial q}-\frac{M_\odot}{L_\odot}\left(\frac{\mu}{\lambda}\right)^{1/2}(\epsilon+\epsilon_\nu+\epsilon_{\mathrm{g}})\frac{\psi}{\theta}, \tag{9d}$$

$$0=\frac{\partial\mu}{\partial q}-\frac{\psi}{\theta}, \tag{9e}$$

$$0=\frac{\partial\psi}{\partial q}, \tag{9f}$$

$$0=\frac{\partial X_i}{\partial t}+\frac{2}{3M_\odot\mu^{1/2}}\frac{\partial F_i}{\partial\mu}-\Psi_i(\xi,\eta,\boldsymbol{X}), 1\leq i\leq n_{\mathrm{elem}}. \tag{9g}$$

These equations are solved simultaneously with boundary conditions-at the center:

$$\zeta(1,t)=0,\quad \lambda(1,t)=0,\quad \mu(1,t)=0, \tag{10}$$

and at the surface:

$$\xi(n,t)=\xi_{\mathrm{atm}}(L_\star,R_\star,t),\quad \eta(n,t)=\eta_{\mathrm{atm}}(L_\star,R_\star,t),\quad \mu(n,t)=\mu_{\mathrm{atm}}, \tag{11}$$

along with constitutive relations (e.g., equations of state, opacity laws) to evolve the stellar model in time.

4.2.4 Input physics

The models are computed for 1D, single stars without rotation, magnetic fields, or diffusion. Mass loss is not considered in this project; the only mechanism that alters the stellar mass is accretion. The initial chemical composition follows the solar mixture of Asplund et al. (2009), as recommended by Serenelli et al. (2009), with the exception of the deuterium abundance, which is varied to explore its impact on accreting stars.

Convection is modeled using mixing-length theory (MLT) (Cox and Giuli 1968), with no overshooting. We adopt the solar-calibrated value of the mixing-length parameter, $\alpha_{\mathrm{MLT}}=1.64$, and apply the Schwarzschild criterion to determine convective boundaries.

The equation of state (EoS) and opacity are interpolated from the OPAL2005 tables (Iglesias and Rogers 1996; Rogers and Nayfonov 2002; Rogers and Iglesias 1992), and supplemented at low temperatures by the AF opacity tables (Ferguson et al. 2005). Nuclear reaction rates are based on NACRE (Aikawa et al. 2006) and LUNA (Broggini et al. 2018) tables. The models include the full PP and CNO cycles, tracking the evolution of abundances for ^{1}H, ^{2}H, ^{3}He, ^{4}He, ^{7}Li, ^{7}Be, ^{12}C, ^{13}C, ^{14}N, ^{15}N, ^{16}O, ^{17}O.

Neutrino energy losses are treated using the prescriptions of Haft et al. (1994) for plasma neutrinos and Weigert (1966) for photoneutrinos. The atmosphere is implemented via a Hopf $T(\tau)$ relation from Hubeny and Mihalas (2015), with a maximum optical depth of $\tau_{\mathrm{max}}=20$.

The input physics are summarized in Table 1. Building on this framework, we next describe the implementation of accretion in `Cesam2k20`.

Parameter Type	Description
Mass	accretion + no mass loss
Chemical composition	AGS09+S10[1]
Convection	MLT[2] + No overshoot
Diffusion	None
EoS	OPAL2005[3]
Opacity	OPAL and AF [4]
Nuclear reaction	NACRE + LUNA[5]
Atmosphere	Hopf[6], $\tau_{\max} = 20.0$

Table 1: Summary of input parameters for Cesam2k20 models; refer to the text for more details.

4.3 Accretion in `Cesam2k20`

4.3.1 Limiting the maximum change in gravitational energy

4.3.2 Limiting the maximum change in mass

5 Results

5.1 The toy problem

- the toy problem of static models, without accretion but differe slightly in mass to emulate the effect of accretion
- one with full convective stars and the other with radiative core
- ? the profile of the gravitational energy and the heat from accretion
- show the problem with this kind of approach necessicate the implementation of accretion in the actual evolution
- can also show the entropy profile inside to star to illustrate the problem of discountinuity

5.2 The effect of different accretion rates

5.3 The effect of different chemical compositions

- compare accreting models with and without deuterium accreted in the outer layers
- can try to vary the abundance of deuterium in the accreted material

5.4 Comparison with Palla & Stahler (1993)

6 Conclusion

- summarize the main findings of the project
- discuss the limitations and prospects of this research

- limitations of the current implementation
  - the seed mass is $0.1M_{\odot}$ can be smaller
  - angular momentum is not considered
  - variable accretion rate
  - numeircal treatment of convective-radiative boundary
  - hot/cold accretion

References

Aikawa, M. et al. (2006). "NACRE Update and Extension Project". In: Frontiers in Nuclear Structure, Astrophysics, and Reactions. Vol. 831. AIP, pp. 26–30. DOI: 10.1063/1.2200894.

Alencar, S. H. P. et al. (2012). "Accretion Dynamics in the Classical T Tauri Star V2129 Ophiuchi". In: *Astronomy and Astrophysics* 541, A116. DOI: 10.1051/0004-6361/201118395.

Asplund, M. et al. (2009). "The Chemical Composition of the Sun". In: *Annual Review of Astronomy and Astrophysics* 47 (Volume 47, 2009), pp. 481–522. DOI: 10.1146/annurev.astro.46.060407.145222.

Bally, J. (2016). "Protostellar Outflows". In: *Annual Review of Astronomy and Astrophysics* 54, pp. 491–528. DOI: 10.1146/annurev-astro-081915-023341.

Baraffe, I., G. Chabrier, and J. Gallardo (2009). "Episodic Accretion at Early Stages of Evolution of Low-Mass Stars and Brown Dwarfs: A Solution for the Observed Luminosity Spread in H-R Diagrams?" In: *The Astrophysical Journal* 702, pp. L27–L31. DOI: 10.1088/0004-637X/702/1/L27.

Baraffe, I., E. Vorobyov, and G. Chabrier (2012). "Observed Luminosity Spread in Young Clusters and FU Ori Stars: A Unified Picture". In: *The Astrophysical Journal* 756, p. 118. DOI: 10.1088/0004-637X/756/2/118.

Bouvier, J. (2014). "The Magnetospheric Accretion/Ejection Process in Young Stellar Objects: Open Issues and Perspectives". In: European Physical Journal Web of Conferences. Vol. 64. eprint: arXiv:1310.4439, p. 09001. DOI: 10.1051/epjconf/20136409001.

Bouvier, J. et al. (2007). *Magnetospheric Accretion in Classical T Tauri Stars*. DOI: 10.48550/arXiv.astro-ph/0603498. URL: https://ui.adsabs.harvard.edu/abs/2007prpl.conf..479B. Pre-published.

Broggini, C. et al. (2018). "LUNA: Status and Prospects". In: *Progress in Particle and Nuclear Physics* 98, pp. 55–84. DOI: 10.1016/j.ppnp.2017.09.002.

Cox, J. P. and R. T. Giuli (1968). *Principles of Stellar Structure*.

Eggleton, P. P. (1971). "The Evolution of Low Mass Stars". In: *Monthly Notices of the Royal Astronomical Society* 151, p. 351. DOI: 10.1093/mnras/151.3.351.

Ferguson, J. W. et al. (2005). "Low-Temperature Opacities". In: *The Astrophysical Journal* 623, pp. 585–596. DOI: 10.1086/428642.

Guillot, T. and P. Morel (1995). "CEPAM: A Code for Modeling the Interiors of Giant Planets." In: *Astronomy and Astrophysics Supplement Series* 109, pp. 109–123.

Haft, M., G. Raffelt, and A. Weiss (1994). "Standard and Nonstandard Plasma Neutrino Emission Revisited". In: *The Astrophysical Journal* 425, p. 222. DOI: 10.1086/173978.

Hartmann, L., G. Herczeg, and N. Calvet (2016). "Accretion onto Pre-Main-Sequence Stars". In: *Annual Review of Astronomy and Astrophysics* 54 (Volume 54, 2016), pp. 135–180. DOI: 10.1146/annurev-astro-081915-023347.

Hayashi, C. (1961). "Stellar Evolution in Early Phases of Gravitational Contraction." In: *Publications of the Astronomical Society of Japan* 13, pp. 450–452.

Henyey, L. G., R. Lelevier, and R. D. Levée (1955). "The Early Phases of Stellar Evolution". In: *Publications of the Astronomical Society of the Pacific* 67, p. 154. DOI: 10.1086/126791.

Herbst, W. et al. (2007). *The Rotation of Young Low-Mass Stars and Brown Dwarfs*. DOI: 10.48550/arXiv.astro-ph/0603673. URL: https://ui.adsabs.harvard.edu/abs/2007prpl.conf..297H (visited on 06/10/2025). Pre-published.

Hosokawa, T., S. S. R. Offner, and M. R. Krumholz (2011). "On the Reliability of Stellar Ages and Age Spreads Inferred from Pre-main-sequence Evolutionary Models". In: *The Astrophysical Journal* 738, p. 140. DOI: 10.1088/0004-637X/738/2/140.

Hubeny, I. and D. Mihalas (2015). *Theory of Stellar Atmospheres. An Introduction to Astrophysical Non-equilibrium Quantitative Spectroscopic Analysis*.

Iglesias, C. A. and F. J. Rogers (1996). "Updated Opal Opacities". In: *The Astrophysical Journal* 464, p. 943. DOI: 10.1086/177381.

Ireland, L. G. et al. (2020). "Magnetic Braking of Accreting T Tauri Stars: Effects of Mass Accretion Rate, Rotation, and Dipolar Field Strength". In: *The Astrophysical Journal* 906.1, p. 4. DOI: 10.3847/1538-4357/abc828.

Kastner, J. H. et al. (2002). "Evidence for Accretion: High-Resolution X-Ray Spectroscopy of the Classical T Tauri Star TW Hydrae". In: *The Astrophysical Journal* 567, pp. 434–440. DOI: 10.1086/338419.

Kippenhahn, R., A. Weigert, and A. Weiss (2013). *Stellar Structure and Evolution*. DOI: 10.1007/978-3-642-30304-3.

Koenigl, A. (1991). "Disk Accretion onto Magnetic T Tauri Stars". In: *The Astrophysical Journal* 370, p. L39. DOI: 10.1086/185972.

Kunitomo, M. and T. Guillot (2021). "Imprint of Planet Formation in the Deep Interior of the Sun". In: *Astronomy & Astrophysics* 655, A51. DOI: 10.1051/0004-6361/202141256.

Kunitomo, M. et al. (2017). "Revisiting the Pre-Main-Sequence Evolution of Stars - I. Importance of Accretion Efficiency and Deuterium Abundance". In: *Astronomy & Astrophysics* 599, A49. DOI: 10.1051/0004-6361/201628260.

Larson, R. B. (1969). "Numerical Calculations of the Dynamics of Collapsing Proto-Star". In: *Monthly Notices of the Royal Astronomical Society* 145, p. 271. DOI: 10.1093/mnras/145.3.271.

Lii, P. S. et al. (2014). "Propeller-Driven Outflows from an MRI Disc". In: *Monthly Notices of the Royal Astronomical Society* 441.1, pp. 86–100. DOI: 10.1093/mnras/stu495.

Manchon, L. (2021). "On the Transport of Angular Momentum in Stellar Radiative Zones in 2D". PhD thesis. Université Paris-Saclay.

Marques, J. P. et al. (2013). "Seismic Diagnostics for Transport of Angular Momentum in Stars. I. Rotational Splittings from the Pre-Main Sequence to the Red-Giant Branch". In: *Astronomy and Astrophysics* 549, A74. DOI: 10.1051/0004-6361/201220211.

Morel, P. (1997). "CESAM: A Code for Stellar Evolution Calculations". In: *Astronomy and Astrophysics Supplement Series* 124, pp. 597–614. DOI: 10.1051/aas:1997209.

Morel, P. and Y. Lebreton (2008). "CESAM: A Free Code for Stellar Evolution Calculations". In: *Astrophysics and Space Science* 316, pp. 61–73. DOI: 10.1007/s10509-007-9663-9.

Muzerolle, J., N. Calvet, and L. Hartmann (2001). "Emission-Line Diagnostics of T Tauri Magnetospheric Accretion. II. Improved Model Tests and Insights into Accretion Physics". In: *The Astrophysical Journal* 550, pp. 944–961. DOI: 10.1086/319779.

Palla, F. and S. W. Stahler (1993). "The Pre-Main-Sequence Evolution of Intermediate-Mass Stars". In: *The Astrophysical Journal* 418, p. 414. DOI: 10.1086/173402.

Press, W. H. et al. (1992). *Numerical Recipes in FORTRAN. The Art of Scientific Computing*.

Rogers, F. J. and A. Nayfonov (2002). "Updated and Expanded OPAL Equation-of-State Tables: Implications for Helioseismology". In: *The Astrophysical Journal* 576, pp. 1064–1074. DOI: 10.1086/341894.

Rogers, F. J. and C. A. Iglesias (1992). “Rosseland Mean Opacities for Variable Compositions”. In: *The Astrophysical Journal* 401, p. 361. DOI: 10.1086/172066.

Romanova, M. M. et al. (2004). “The Propeller Regime of Disk Accretion to a Rapidly Rotating Magnetized Star”. In: *The Astrophysical Journal* 616.2, p. L151. DOI: 10.1086/426586.

Serenelli, A. M. et al. (2009). “NEW SOLAR COMPOSITION: THE PROBLEM WITH SOLAR MODELS REVISITED”. In: *The Astrophysical Journal* 705.2, p. L123. DOI: 10.1088/0004-637X/705/2/L123.

Stelzer, B. and R. Neuhäuser (2001). “X-Ray Emission from Young Stars in Taurus-Auriga-Perseus: Luminosity Functions and the Rotation - Activity - Age - Relation”. In: *Astronomy and Astrophysics* 377, pp. 538–556. DOI: 10.1051/0004-6361:20011093.

Weigert, A. (1966). “Sternentwicklung VI: Entwicklung Mit Neutrinoverlusten Und Thermische Pulse Der Helium-Schalenquelle Bei Einem Stern von 5 Sonnenmassen”. In: *Zeitschrift fur Astrophysik* 64, p. 395.

A Appendix: The jacobian of the stellar structure equations